# Active tuning of mid-infrared metamaterials by electrical control of carrier densities

**Young Chul Jun,[1,*] Edward Gonzales,[1] John L. Reno,[1] Eric A. Shaner,[2] Alon Gabbay,[1] and Igal Brener[1,2]**

[1]*Center for Integrated Nanotechnologies (CINT), Sandia National Laboratories, P.O. Box 5800, Albuquerque, New Mexico 87185, USA*

[2]*Sandia National Laboratories, P.O. Box 5800, Albuquerque, New Mexico 87185, USA*

** youngchul.jun@sandia.gov*

**Abstract:** We demonstrate electrically-controlled active tuning of mid-infrared metamaterial resonances using depletion-type devices. The depletion width in an n-doped GaAs epilayer changes with an electric bias, inducing a change of the permittivity of the substrate and leading to frequency tuning of the resonance. We first present our detailed theoretical analysis and then explain experimental data of bias-dependent metamaterial transmission spectra. This electrical tuning is generally applicable to a variety of infrared metamaterials and plasmonic structures, which can find novel applications in chip-scale active infrared devices.



**OCIS codes:** (160.3918) Metamaterials; (130.0250) Optoelectronics; (130.3120) Integrated optics devices; (130.3060) Infrared.

## References and links

1. D. R. Smith, J. B. Pendry, and M. C. K. Wiltshire, "Metamaterials and negative refractive index," Science **305**(5685), 788–792 (2004).
2. V. M. Shalaev, "Optical negative-index metamaterials," Nat. Photonics **1**(1), 41–48 (2007).
3. W. Cai and V. M. Shalaev, *Optical Metamaterials: Fundamentals and Applications* (Springer, 2009).
4. Y. Liu and X. Zhang, "Metamaterials: a new frontier of science and technology," Chem. Soc. Rev. **40**(5), 2494–2507 (2011).
5. N. I. Zheludev, "A roadmap for metamaterials," Opt. Photonics News **22**(3), 30–35 (2011).
6. C. M. Soukoulis and M. Wegener, "Past achievements and future challenges in the development of three-dimensional photonic metamaterials," Nat. Photonics **5**, 523–530 (2011).
7. H. Tao, A. C. Strikwerda, K. Fan, W. J. Padilla, X. Zhang, and R. D. Averitt, "Reconfigurable terahertz metamaterials," Phys. Rev. Lett. **103**(14), 147401 (2009).
8. I. M. Pryce, K. Aydin, Y. A. Kelaita, R. M. Briggs, and H. A. Atwater, "Highly strained compliant optical metamaterials with large frequency tunability," Nano Lett. **10**(10), 4222–4227 (2010).
9. D. H. Werner, D.-H. Kwon, I. C. Khoo, A. V. Kildishev, and V. M. Shalaev, "Liquid crystal clad near-infrared metamaterials with tunable negative-zero-positive refractive indices," Opt. Express **15**(6), 3342–3347 (2007).
10. M. J. Dicken, K. Aydin, I. M. Pryce, L. A. Sweatlock, E. M. Boyd, S. Walavalkar, J. Ma, and H. A. Atwater, "Frequency tunable near-infrared metamaterials based on $VO_2$ phase transition," Opt. Express **17**(20), 18330–18339 (2009).
11. T. Driscoll, H.-T. Kim, B.-G. Chae, B.-J. Kim, Y.-W. Lee, N. M. Jokerst, S. Palit, D. R. Smith, M. Di Ventra, and D. N. Basov, "Memory metamaterials," Science **325**(5947), 1518–1521 (2009).
12. E. Kim, Y. R. Shen, W. Wu, E. Ponizovskaya, Z. Yu, A. M. Bratkovsky, S.-Y. Wang, and R. S. Williams, "Modulation of negative index metamaterials in the near-IR range," Appl. Phys. Lett. **91**(17), 173105 (2007).
13. D. J. Cho, W. Wu, E. Ponizovskaya, P. Chaturvedi, A. M. Bratkovsky, S.-Y. Wang, X. Zhang, F. Wang, and Y. R. Shen, "Ultrafast modulation of optical metamaterials," Opt. Express **17**(20), 17652–17657 (2009).
14. H.-T. Chen, W. J. Padilla, J. M. Zide, A. C. Gossard, A. J. Taylor, and R. D. Averitt, "Active terahertz metamaterial devices," Nature **444**(7119), 597–600 (2006).
15. B. S. Passmore, D. G. Allen, S. R. Vangala, W. D. Goodhue, D. Wasserman, and E. A. Shaner, "Mid-infrared doping tunable transmission through subwavelength metal hole arrays on InSb," Opt. Express **17**(12), 10223–10230 (2009).
16. X. Miao, B. Passmore, A. Gin, W. Langston, S. Vangala, W. Goodhue, E. Shaner, and I. Brener, "Doping tunable resonance: Toward electrically tunable mid-infrared metamaterials," Appl. Phys. Lett. **96**(10), 101111 (2010).

#158883 - $15.00 USD Received 28 Nov 2011; revised 2 Jan 2012; accepted 5 Jan 2012; published 12 Jan 2012

17. K. Anglin, T. Ribaudo, D. C. Adams, X. Qian, W. D. Goodhue, S. Dooley, E. A. Shaner, and D. Wasserman, "Voltage-controlled active mid-infrared plasmonic devices," J. Appl. Phys. **109**(12), 123103 (2011).
18. M. Osawa, "Surface-enhanced infrared absorption," in *Near-Field Optics and Surface Plasmon Polaritons*, S. Kawata, ed. (Springer-Verlag, 2001). p. 163.
19. M. Vollmer and K.-P. Möllmann, *Infrared Thermal Imaging: Fundamentals, Research, and Applications* (Wiley-VCH, 2010).
20. R. Martini, C. Gmachl, J. Falciglia, F. G. Curti, C. G. Bethea, F. Capasso, E. A. Whittaker, R. Paiella, A. Tredicucci, A. L. Hutchinson, D. L. Sivco, and A. Y. Cho, "High-speed modulation and free-space optical audio/video transmission using quantum cascade lasers," Electron. Lett. **37**(3), 191–193 (2001).
21. C. Kittel, *Introduction to Solid State Physics*, 7th ed. (Wiley, 1995).
22. "Semiconductors on NSM," http://www.ioffe.ru/SVA/NSM/Semicond/.
23. A. Raymond, J. L. Robert, and C. Bernard, "The electron effective mass in heavily doped GaAs," J. Phys. C Solid State Phys. **12**(12), 2289–2293 (1979).
24. M. Cardona, "Electron effective masses of InAs and GaAs as a function of temperature and doping," Phys. Rev. **121**(3), 752–758 (1961).
25. J. S. Blakemore, "Semiconducting and other major properties of gallium arsenide," J. Appl. Phys. **53**(10), R123–R181 (1982).
26. R. F. Pierret, *Semiconductor Device Fundamentals* (Addison Wesley, 1996)
27. Lumerical Simulations, http://www.lumerical.com
28. E. D. Palik, *Handbook of Optical Constants and Solids* (Academic, 1985).
29. D. Schurig, J. J. Mock, and D. R. Smith, "Electric-field-coupled resonators for negative permittivity metamaterials," Appl. Phys. Lett. **88**(4), 041109 (2006).
30. C. J. Sandroff, R. N. Nottenburg, J.-C. Bischoff, and R. Bhat, "Dramatic enhancement in the gain of a GaAs/AlGaAs heterostructure bipolar transistor by surface chemical passivation," Appl. Phys. Lett. **51**(1), 33–35 (1987).
31. T. Ohno, "Sulfur passivation of GaAs surfaces," Phys. Rev. B Condens. Matter **44**(12), 6306–6311 (1991).
32. E. A. Shaner, J. G. Cederberg, and D. Wasserman, "Electrically tunable extraordinary optical transmission gratings," Appl. Phys. Lett. **91**(18), 181110 (2007).

## 1. Introduction

There has recently been tremendous interest in the development of optical metamaterials (MMs). Artificially tailored electromagnetic structures can exhibit exotic optical properties such as optical magnetism, negative refraction, sub-diffraction imaging, and cloaking [1–6]. Active tuning of MMs is emerging as a natural next step in this burgeoning field. Tunable MMs also have potential for novel active devices such as optical switches, modulators, filters, and phase shifters. There have been several approaches for active tuning - e.g. with mechanical movement or stretching [7,8], reorientation in liquid crystals [9], phase transitions in vanadium dioxide ($VO_2$) [10,11], and optical modulation of material properties [12,13]. However, electrical control based on semiconductor device structures is more technologically appealing for practical, chip-scale devices.

Electrically-controlled active tuning of MMs was first demonstrated at terahertz (THz) frequencies [14]. The free carrier absorption in a doped-GaAs substrate was dynamically controlled with an electric bias, by changing the carrier concentration in the substrate. This causes a strong amplitude modulation (~50%). However, at higher frequencies (such as mid-IR), the free carrier absorption is much smaller and it cannot be modulated in such a way. Thus, this amplitude tuning cannot be simply translated into the mid-IR region.

Despite this, there have been efforts to induce spectral tuning of mid-IR plasmonic and metamaterial resonances using highly-doped semiconductor layers [15–17]. Previously, we showed that the resonant *frequencies* of metallic split-ring resonators (SRRs) can be tuned, depending on semiconductor doping levels [16]. While that work employed separate samples with different doping levels, we demonstrate in this paper *active tuning* of a mid-IR MM resonance with an electric bias voltage. The SRR arrays work as an optical MM layer and electrical metal gate simultaneously. With a reverse bias applied to the metal gate, the refractive index of the substrate directly underneath the metallic resonators varies through changes in the depletion width in a highly doped semiconductor. This results in frequency tuning of MM resonances rather than amplitude tuning. This technique can be applied to a variety of infrared metamaterials and plasmonic structures. The mid-IR spectral range is

#158883 - $15.00 USD Received 28 Nov 2011; revised 2 Jan 2012; accepted 5 Jan 2012; published 12 Jan 2012

technologically important for a number of applications, including chemical/biological sensing [18], thermal imaging [19], and free-space optical communication [20]. A semiconductor-based approach to active tuning is also appealing as it can be integrated with the fabrication of infrared devices.

The schematic of our device is shown in Fig. 1. The SRRs are connected to an electrical bus line (i.e. horizontal lines) and work as an electrical gate too. They are placed on top of an n + doped GaAs layer and form a metal-semiconductor junction. We need a highly doped n + layer in order to induce a large dielectric constant change. We also include an insulating barrier (i.e. undoped 30 nm $Al_{0.3}Ga_{0.7}As$ layer) to reduce leakage current. The gold SRR is designed to be resonant in the mid-IR ($\lambda_0$ ~10 μm). The transmission spectrum through the MM layer shows a dip at the resonance frequency. By applying an electric bias and changing the depletion width in the substrate, we dynamically tune the frequency of this transmission minimum.

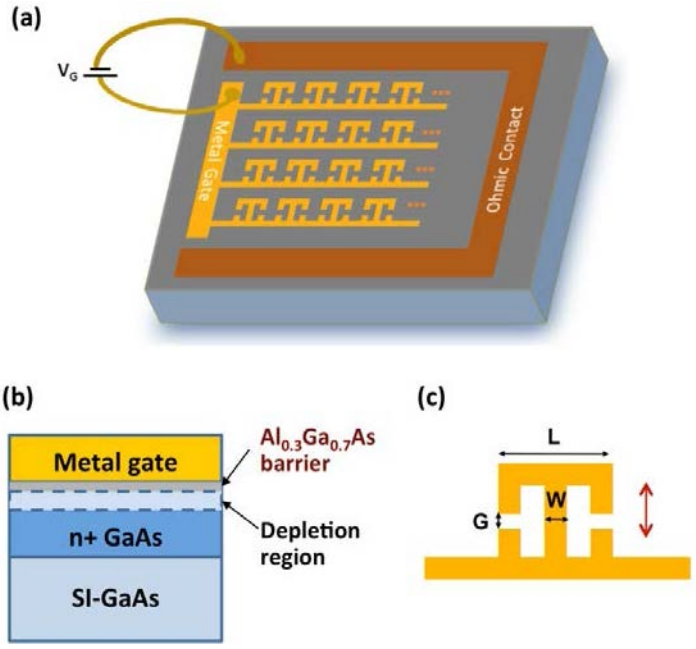


Fig. 1. (a) Schematic of the device. (b) Diagram of the substrate and the depletion region in the metal-semiconductor junction. (c) Geometry of the modified split-ring resonator and the electrical bus line: L = 720 nm, W = 130 nm, G = 110 nm. The gold SRR thickness is 60 nm. The polarization of incident light is indicated by the red arrow.

## 2. Theory

First, we theoretically analyze our device operation. The dielectric constant ε of a semiconductor substrate can be modeled using the Drude approximation [21]:

$$\varepsilon = \varepsilon_\infty \left(1 - \frac{\omega_p^2}{\omega^2 + i\omega\Gamma}\right) = \varepsilon_\infty \left(1 - \frac{\omega_p^2}{\omega^2 + \Gamma^2} + i\frac{\omega_p^2\Gamma}{\omega(\omega^2 + \Gamma^2)}\right) \quad (1)$$

where $\varepsilon_\infty$ is the high frequency dielectric constant, ω is the angular frequency. Here, the plasma frequency $\omega_p$ and the relaxation frequency Γ (i.e. damping term) are given by

$$\omega_p^2 = \frac{Nq^2}{\varepsilon_0 \varepsilon_\infty m^*} \quad (2)$$

#158883 - $15.00 USD Received 28 Nov 2011; revised 2 Jan 2012; accepted 5 Jan 2012; published 12 Jan 2012

and

$$\Gamma = 1/\tau = \frac{q}{\mu m^*} \tag{3}$$

where τ is the scattering time, m* is the electron effective mass, μ is the electron mobility, q is the electron charge, and N is the electron density (which is the same as the doping level $N_D$, assuming full ionization of dopants).

Here, we should note that the electron effective mass m* and mobility μ also vary with the carrier density N. We obtained experimental values for the carrier concentration dependent effective mass and mobility of GaAs from literature [22–24] and calculated the dielectric constant as a function of the doping level.

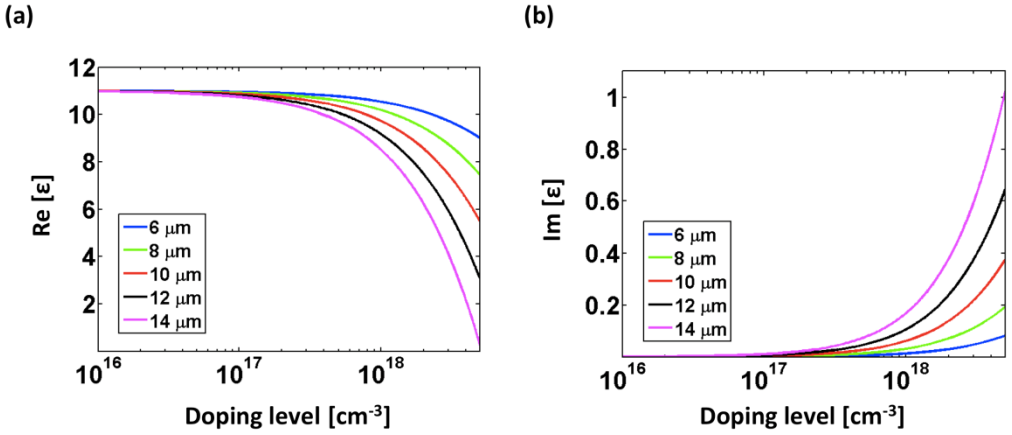


Fig. 2. Drude model calculations of dielectric constants in n-doped GaAs (for several mid-IR wavelengths). (a) is the real part and (b) is the imaginary part of the dielectric constant.

Figure 2 shows the calculated dielectric constant (real and imaginary parts) of n-doped GaAs for several mid-IR wavelengths. In the high doping region (>$N_D$ = $10^{18}$ $cm^{-3}$), the dielectric constant decreases rapidly. So, starting from an n + GaAs doped layer ($N_D$ = 5 x $10^{18}$ $cm^{-3}$), we can remove carriers with an electric bias (by increasing the depletion region width) and obtain large dielectric constant change Δε ~5.5 at $\lambda_0$ = 10 μm. Such a change becomes more significant at longer wavelengths. However, the imaginary part of dielectric constant also increases rapidly (i.e. it becomes lossy) at longer wavelengths. The real part of dielectric constant eventually becomes negative (Re[ε] < 0) at very large doping levels. We also notice that the dielectric constant change is very small at shorter wavelengths (e.g. near-IR).

From these calculations, we actually find that the damping constant Γ is an order of magnitude smaller than ω in the mid-IR because the electron mobility of GaAs is fairly high: ω = 1.88 x $10^{14}$ $s^{-1}$ (at $\lambda_0$ = 10 μm) and Γ ≈ 3.28 x $10^{12}$ $s^{-1}$ (using μ = 8000 $cm^2/V{\cdot}s$). (The mobility μ decreases at high doping levels, but ω is still an order of magnitude larger than Γ) Thus, Eq. (1) can be further simplified to

$$\varepsilon(\omega) = \mathrm{Re}[\varepsilon(\omega)] + \mathrm{Im}[\varepsilon(\omega)] \approx \varepsilon_\infty \left(1 - \frac{\omega_p^2}{\omega^2} + i\frac{\omega_p^2}{\omega^3}\Gamma\right) \tag{4}$$

Because the plasma frequency $\omega_p$ is inversely proportional to the effective mass, we expect a larger change in the real part of the dielectric constant for a substrate with a smaller effective mass. For example, n-type doping in GaAs is more favorable than p-type doping because of the smaller electron effective mass ($m_e^*$ = 0.067$m_0$) than the hole effective mass ($m_{hh}^*$ = 0.52$m_0$). It is also known that the electron effective masses of III-V semiconductors

#158883 - $15.00 USD Received 28 Nov 2011; revised 2 Jan 2012; accepted 5 Jan 2012; published 12 Jan 2012

are not affected much by temperature [24,25], so we expect similar dielectric constant (real part) changes even at cryogenic temperatures.

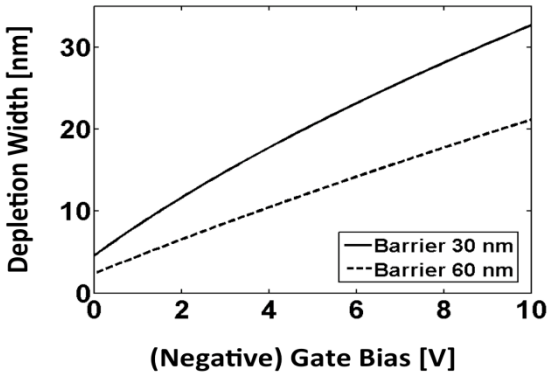


Fig. 3. Depletion width change as a function of the reverse gate bias. We assume a $Al_{0.3}Ga_{0.7}As$ barrier. We also plot for a thicker barrier (dotted line) for comparison. The doping level of the n + GaAs epilayer is $N_D = 5 \times 10^{18}$ $cm^{-3}$.

The depletion width changes in an n-doped GaAs can be estimated using a textbook formula for a MIS (metal-insulator-semiconductor) capacitor [26]:

$$W_{depletion} = \left[ \frac{2\varepsilon_{GaAs}\varepsilon_0}{qN_D}(-\phi_s) \right]^{1/2} \tag{5}$$

where the surface potential $_s$ is related to the gate voltage $V_G$ as follows:

$$V_G = \phi_s - \frac{\varepsilon_{GaAs}}{\varepsilon_{AlGaAs}} W_{barrier} \left[ \frac{2qN_D}{\varepsilon_{GaAs}\varepsilon_0} |\phi_s| \right]^{1/2} + \phi_{MS} \tag{6}$$

Here, $\phi_{MS}$ is the flat-band voltage (i.e. a work function difference of metal and GaAs). Note that dielectric constants we use here are the static values ($\varepsilon_{GaAs} = 12.9$ and $\varepsilon_{Al0.3Ga0.7As} = 12.05$) [23], not the high frequency ones.

The calculated depletion width change is plotted in Fig. 3. With a negative bias, the depletion width increases by tens of nm. An ideal MIS capacitor has an inversion threshold voltage, beyond which the depletion growth stops and minority carriers (i.e. holes) appear at the insulator-semiconductor interface. Because our active tuning depends on depletion width changes, this pinning of depletion width is not desirable. Technically, this inversion can be avoided by using a pulsed or modulated bias (inducing 'deep depletion'). However, we expect that minority carriers can leak through our relatively thin, low-height $Al_{0.3}Ga_{0.7}As$ barrier. So, the strong inversion is not likely to occur in an actual device. The depletion widths in Fig. 3 were also verified by numerical calculations using a semiconductor device simulator.

Finally, we estimated the MM resonance shifts with numerical simulations. We performed FDTD (finite difference time domain) simulations [27] which include structures shown in Fig. 1. We employed a different depletion width for each bias and repeated the FDTD simulations. The depletion region in the actual device grows in all directions around a metal gate (generating cylindrical or spherical region of carrier depletion). Because we use rectangular grids in our 3-dimensional FDTD simulations, we will need a very small grid size and have huge computational loads if we include such small cylindrical or spherical regions in our simulation domain. Instead, we modeled the depletion region as a thin, planar layer underneath the metamaterial gate. The metamaterial field exponentially decays in the

#158883 - $15.00 USD Received 28 Nov 2011; revised 2 Jan 2012; accepted 5 Jan 2012; published 12 Jan 2012

substrate and the part of this field interacts with the depletion region. We believe this is a good modeling in consideration of both computational load and accuracy.

The wavelength-dependent dielectric constants from the Drude model (Fig. 2) were used for the n + GaAs epilayer. (This is an approximation, but note that the Drude model with a damping term is usually used for modeling dispersive materials in FDTD simulations) The dielectric constants for gold and undoped layers are obtained from literature [28]. Our FDTD simulation includes a unit cell of SRR and electrical bus line. The dimensions of the structure are given in Fig. 1(c). The SRR geometry was chosen to have a resonance around 1000 $cm^{-1}$ ( = 10 μm, note that wavenumber [$cm^{-1}$] = 10000 / λ [μm]). We chose a modified SRR geometry (which is an electrical metamaterial [29]) as our "meta-atom" because of its strong field enhancement in two gaps and the easiness for electrical connection; other MM geometries can be used too. We used periodic boundary conditions in the MM plane and the perfectly matching layers in the other directions normal to the MM plane. The period between SRRs was 2 μm. A broadband light pulse was incident from top (normal to the MM plane) and polarized orthogonal to the SRR gap (i.e. red arrow in Fig. 1(c)) to excite a LC resonance in the SRR. The transmission was measured in the substrate side.

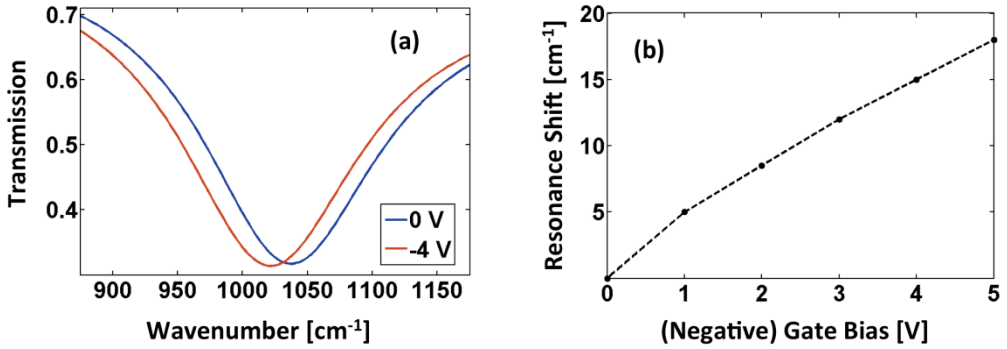


Fig. 4. (a) Metamaterial transmission spectra obtained from FDTD simulations for the gate bias $V_G$ = 0 V and –4 V. (b) Resonance red-shift as a function of a reverse bias to the gate.

Figure 4(a) shows the obtained transmission resonance spectra for $V_G$ = 0 V and –4 V. The transmission dip exhibits a spectral shift with a bias. The resonance spectrum gradually red-shifts with an increased reverse bias (Fig. 4(b)). This red-shift can be understood from a capacitor model. Because the resonance frequency in these resonators is proportional to $\omega_0 \alpha 1/\sqrt{c}$, we have $\omega_0 1/\sqrt{c} = 1/n$ (from $C = \varepsilon d / A$), where n is the refractive index of a substrate. When the depletion width increases, the substrate refractive index increases (Fig. 2(a)) and the resonance red-shifts. The shift is relatively small, but still large enough to be clearly observed in a real device.

### 3. Device fabrication

For the experimental study, we fabricated a gold MM layer on GaAs epilayers together with metal contacts. Figure 5 shows the images of the fabricated device. An undoped GaAs buffer layer and a 700 nm thick n + GaAs epilayer ($N_D$ = 5 x $10^{18}$ $cm^{-3}$) were grown on a semi-insulating GaAs substrate by molecular beam epitaxy, followed by the growth of a 30 nm undoped $Al_{0.3}Ga_{0.7}As$ barrier layer and a 5 nm GaAs cap layer (see Fig. 1(b)). First, metal contacts were defined by optical lithography, metal deposition, and lift-off processes (Fig. 5(a)). The larger outside ohmic contact was fabricated by electron-beam deposition of Ge (26 nm) / Au (54 nm) / Ni (14 nm) / Au (150 nm) in sequence and then by rapid thermal annealing at 380 °C for 30 seconds in an Ar atmosphere. Next, the inner metal gate was fabricated by plasma-enhanced chemical vapor deposition (PECVD) of a 70 nm $SiO_2$, followed by electron-beam deposition of Ti (10 nm) / Au (150 nm). The insulating $SiO_2$ film

#158883 - $15.00 USD Received 28 Nov 2011; revised 2 Jan 2012; accepted 5 Jan 2012; published 12 Jan 2012

prevents current flow through the metal gate – i.e. the current flows through only the MM layer. This removes undesirable heating in the metal gate and also makes the interpretation of data easier - and protects the $Al_{0.3}Ga_{0.7}As$ barrier layer from damage during wire-bonding. A 1mm by 1mm MM layer (i.e. SRR arrays) was connected to this metal gate via electrical bus lines (i.e. horizontal lines in Fig. 5(b)).

The SRR arrays were patterned by electron-beam lithography and metal deposition of Ti (5 nm) / Au (60 nm) (see Fig. 5(b) for a SEM image). The dimension of the SRR is given in Fig. 1(c). We used a very large write-field (500 μm x 500 μm) in electron-beam lithography, but it was still smaller than our active area (1 mm x 1 mm). Since stitching between electron beam write-fields could break electrical bus lines, the stage movement during electron-beam writing was carefully controlled to avoid such a problem.

Finally, both ohmic and metal gate contacts were wire-bonded to a chip carrier for electric biasing.

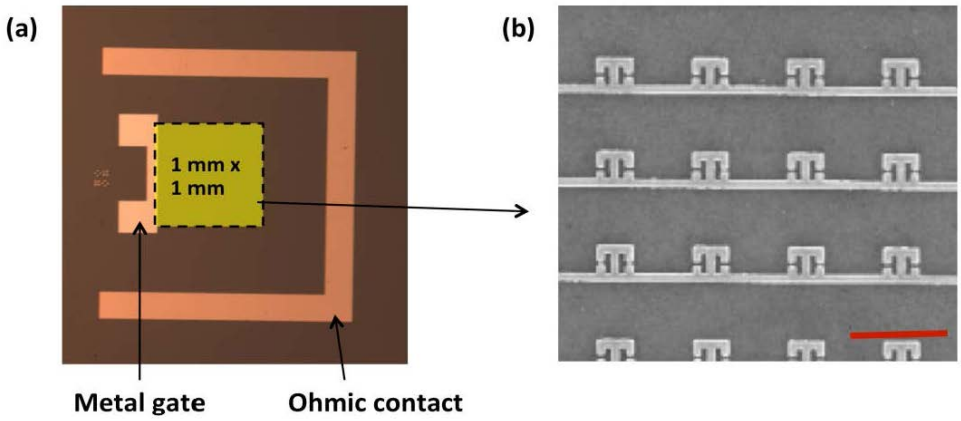


Fig. 5. (a) An optical microscope image of metal contacts (patterned using optical lithography). The outside contact is an ohmic contact, and the inner one is a metal gate contact which is connected to the active area (colored region). The size of the active (SRR) region is 1mm x 1mm. Both metal gate and ohmic contact are later wire-bonded to a chip-carrier for electric biasing. (b) A SEM image of SRR arrays (patterned using electron-beam lithography). The red bar is 2 μm.

## 4. Transmission spectra measurement with an electric bias

Transmission spectra of the fabricated metamaterial devices were measured at room temperature with a Bruker IFS 66v/S Fourier-transform infrared spectrometer (FTIR) using a liquid-nitrogen cooled mercury cadmium telluride (MCT) detector. Incident glow bar emission was polarized normal to the SRR gap. FTIR spectra were referenced to a bare substrate region which did not have metal structures. The sample was biased (DC) using a Keithley 2400 Source meter during transmission measurements.

Figure 6 shows a representative SRR transmission spectrum. As the reverse bias increased from 0 V to –4 V, the resonant transmission peak red-shifted in agreement with theory (Fig. 4(a)). We also measured the resonant frequencies with gradually varying bias voltages. The center frequency was determined by fitting a Gaussian curve to the FTIR spectra. The shift was small, but we can clearly see that it gradually red-shifts with a negative bias (Fig. 7(a)). Figure 7(b) shows the measured IV curve from the same device. It exhibits a diode or Schottky contact behavior (though it has a breakdown at a moderate reverse bias level). The forward bias has much larger current flow than the reverse bias. This IV characteristics implies that the depletion region is formed at the metal-semiconductor junction and its width increases with reverse bias voltages. In agreement with this, we obtained gradually increasing resonance shifts with a bias.

#158883 - $15.00 USD Received 28 Nov 2011; revised 2 Jan 2012; accepted 5 Jan 2012; published 12 Jan 2012

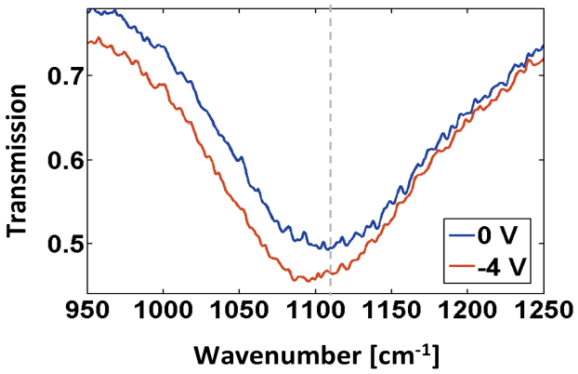


Fig. 6. FTIR measurement of SRR transmission spectra for the gate bias $V_G$ = 0 V and –4 V. The dotted vertical line is the center frequency of $V_G$ = 0 V. We can see that the spectrum at $V_G$ = –4 V is slightly red-shifted.

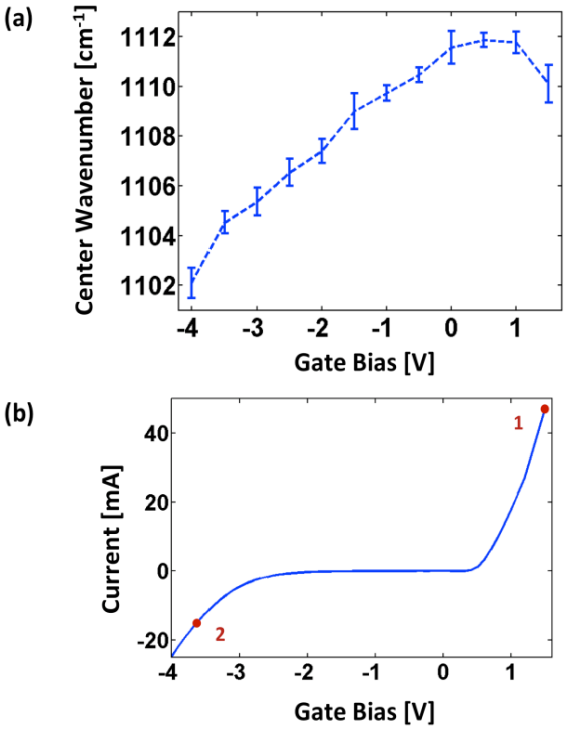


Fig. 7. (a) The center frequency of the metamaterial transmission resonance vs. gate bias. The center frequency was determined by Gaussian fitting. The error bar was obtained from the repetition of measurements. (b) IV curve of the same device. The forward and reverse biases show clearly different behaviors.

We notice that the observed shift is smaller than our theory (Fig. 4(b)). One possible reason for smaller shifts can be smaller depletion widths in the actual device. GaAs often suffers from surface states and Fermi level pinning, which can reduce depletion width changes in a real device. This Fermi level pinning can be possibly relaxed by surface chemical passivation [30,31].

We also observed a small red-shift in the forward bias as well. In the forward bias region, there is no depletion region formed, but large current flows through the device. This large current can induce a slight refractive index change in the substrate by thermal heating [32].

#158883 - $15.00 USD Received 28 Nov 2011; revised 2 Jan 2012; accepted 5 Jan 2012; published 12 Jan 2012

Thermal heating also generates free carriers in the substrate and the whole transmission amplitude can decrease by the increased free carrier absorption. Since under reverse bias the device has leakage current, red-shifts under reverse bias can also have some contribution from thermal heating. However considering power consumption in the device, we can argue that thermal heating was not the dominant mechanism of resonance shifts in our device. For example, let us compare two points $V_1$ = 1.5 V and $V_2$ = −3.7 V. Assuming all voltage drop occurs in the metal-semiconductor junction, we can say that the power consumption in the device is P = VI. Reading the current values from the IV curve ($I_1$ = 47.25 mA, $I_2$ = 16.82 mA), we get the power consumption $P_1$ = 70.9 mW and $P_2$ = 62.2 mW. Although both have similar power consumption (and thus similar amount of thermal heating), the forward bias has much smaller shift: ~1 $cm^{-1}$ at $V_1$, ~8 $cm^{-1}$ at $V_2$. Moreover, we still observe larger red-shifts in smaller reverse bias voltages (< $|V_2|$) in spite of much smaller power consumption. To first order, we can say that the resonance shift difference between these two points $V_1$ and $V_2$ comes from the depletion width difference.

To reduce thermal heating, we conducted the same measurements at low temperature (77 K) (data not shown here). The leakage current under reverse bias was reduced by about half in the considered bias range, but we still observed similar amount of spectral shifts. This further verifies that the depletion width variation and refractive index change are responsible for this resonance tuning.

Tunability can be further increased either by improving the metamaterial part (e.g. optimizing field overlap with the depletion layer) or by improving the semiconductor part (e.g. using a different semiconductor material such as InSb which has a smaller electron effective mass and larger dielectric constant change [16]). The increased tunability would be interesting for e.g. tunable infrared filters. It would be also interesting to combine ultrafast optical measurements of effective refractive indexes [12,13] with electrical biasing. These will be topics of future investigations.

## 5. Conclusion

In this paper, we investigated electrical tuning of mid-infrared metamaterial resonances. The detailed theoretical analysis and experimental data were presented. The observed gradual red-shift with a reverse bias was attributed to the refractive index change in the substrate. Finally, the possible routes for further improvements were discussed. We expect to find this active tuning useful for various mid-infrared applications.

## Acknowledgments

This work was performed, in part, at the Center for Integrated Nanotechnologies, a U.S. Department of Energy, Office of Basic Energy Sciences user facility. Sandia National Laboratories is a multi-program laboratory managed and operated by Sandia Corporation, a wholly owned subsidiary of Lockheed Martin Corporation, for the U.S. Department of Energy's National Nuclear Security Administration under contract DE-AC04-94AL85000.

#158883 - $15.00 USD Received 28 Nov 2011; revised 2 Jan 2012; accepted 5 Jan 2012; published 12 Jan 2012